A NUMERICAL STUDY ON ADHESIVE THICKNESS EFFECT ON BONDED JOINTS USING A MODIFIED FINITE-THICKNESS COHESIVE ELEMENT

C. Sarrado[a*], F. A. Leone[b], A. Turon[a], C. G. Dávila[b]

[a]*AMADE, Universitat de Girona, Campus Montilivi s/n, 17071 Girona (Spain)*
[b]*Structural Mechanics and Concepts Branch, NASA Langley Research Center, MS 190, Hampton, VA 23681-2199 (USA)*
**carlos.sarrado@udg.edu*

Keywords: cohesive elements, progressive damage modeling, adhesives, bonded joints

Abstract
A new cohesive element formulation is proposed for modeling the initial elastic response, softening and failure of finite-thickness adhesives. By decoupling the penalty stiffness of the cohesive zone model formulation and the physical adhesive modulus, the new formulation ensures proper dissipation of fracture energy for mode I, mode II, and mixed-mode loading conditions with any combination of elastic and fracture material properties. Predictions are made using the new element formulation for double cantilever beam, end-notched flexure, mixed-mode bending, and single lap joint specimens with varying adhesive thicknesses. Good correlation between all predictions and experimental results was observed.

1. Introduction

Cohesive zone models are a widely used technique for modeling damage evolution at interfaces within the framework of finite element analysis. Cohesive elements are governed by a traction-separation law that can take different shapes. The simplest traction-separation law is a linear softening law, which needs two material parameters to be defined: the strength and the fracture toughness. The interface strength sets the stress level at which the cohesive element will begin to soften, whereas the fracture toughness is the energy dissipated during the fracture process. Besides these two physical parameters, a penalty stiffness, which sets the stiffness of the undamaged element, needs to be defined to implement the cohesive law in a finite element framework. As the nodes of an undamaged interface are rigidly tied together, the penalty stiffness is taken as a very high numerical parameter to approximate an initially rigid behavior.

Under mixed-mode loading conditions, the strength, the fracture toughness, and the penalty stiffness have to be defined for opening and shear modes, together with a mixed-mode interpolation criterion. However, it was shown by Turon et al. [1] that, under changing mixed-mode conditions [2], the pure-mode strengths, fracture toughnesses and penalty stiffnesses are not independent, and need to fulfill a constraint to ensure proper energy dissipation. Given that the strength and the fracture toughness are physical properties and the penalty stiffness is a numerical parameter, one of the pure-mode penalty stiffnesses can be adjusted to fulfill the

constraint proposed by Turon et al. and ensure the proper energy dissipation without changing any physically measured material properties. Following that strategy, Turon et al. [3] recently proposed a new cohesive formulation.

In the simulation of adhesively bonded joints, the adhesive layer has a finite thickness that in many occasions cannot be neglected. Finite-thickness cohesive elements can be used to simulate adhesive joints by setting the initial stiffness equal to the actual stiffness of the adhesive. Thus, when using finite-thickness cohesive elements, the initial stiffness is no longer a numerical parameter but a material property and, therefore, there is no numerical parameter that can be freely adjusted to satisfy Turon's constraint.

In the present work, a new approach is proposed to fulfill Turon's constraint while using the actual physical properties of the adhesive. The physical moduli of the adhesive and the interface penalty stiffness are decoupled, so that the finite-thickness cohesive element is the result of a zero-thickness cohesive interface embedded within a linear elastic bulk material. The total deformation of the element is the sum of the linear elastic deformation of the bulk and the deformation of the interface due to damage. Turon's constraint can be fulfilled by adjusting one of the interface penalty stiffnesses.

In this paper, a finite-thickness cohesive element formulation based on Turon's et al. [3] formulation is first presented. Next, the formulation is validated by simulating pure-mode and mixed-mode standard fracture toughness tests and comparing their results to Linear Elastic Fracture Mechanics (LEFM) predictions and experimental data available in the literature. The limitations of the formulation in terms of the cohesive element thickness are discussed next. Finally, a Single Lap Joint (SLJ) test with different adhesive thicknesses is simulated and the numerical results are compared against the experimental data. The formulation proposed herein is shown to yield accurate results for both the standard fracture toughness tests, where the adhesive thickness has little effect on the response, and for the SLJ test, where the adhesive thickness has an appreciable effect on the failure load.

2. Finite-thickness cohesive element formulation

2.1. Stiffnesses decoupling and numerical implementation

The finite-thickness cohesive element proposed herein is the result of a zero-thickness interface embedded within a linear elastic bulk material. The total displacement of the element is divided into the linear elastic deformation of the bulk and the deformation of the interface due to damage, as illustrated in Figure 1.

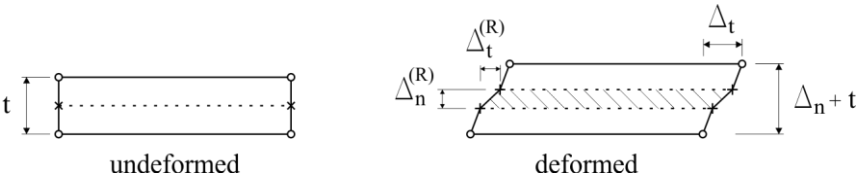

Figure 1. Schematic representation of the decoupling between the bulk adhesive and the embedded interface.

The displacement distribution between the interface and the bulk is proportional to their respective stiffnesses, following the relationship

$$\Delta_n^{(R)} = \Delta_n \frac{K_n}{K_n + K_n^{(\text{int})}\left(1 - d\frac{\langle \Delta_n \rangle}{\Delta_n}\right)} \tag{1}$$

for the opening mode and

$$\Delta_t^{(R)} = \Delta_t \frac{K_t}{K_t + K_t^{(\text{int})}(1-d)} \tag{2}$$

for shear mode, where $\Delta_n^{(R)}$ and $\Delta_t^{(R)}$ are the interface opening and shear displacement jumps, respectively, Δ_n and Δ_t are the element opening and shear displacement jumps, respectively, K_n and K_t are the adhesive opening and shear stiffnesses, respectively, $K_n^{(\text{int})}$ and $K_t^{(\text{int})}$ are the interface opening and shear stiffnesses, respectively, and *d* is the interface damage variable. $\langle x \rangle$ is the Macauley operator, which takes the value of *x* if $x > 0$ and 0 otherwise. The Macauley operator is used to restore the original stiffness in case of interpenetration. The adhesive stiffnesses are computed as

$$K_n = \frac{E_{adh}}{t} \tag{3}$$

$$K_t = \frac{G_{adh}}{t} \tag{4}$$

where E_{adh} and G_{adh} are the adhesive Young's and shear moduli, respectively, and *t* is the adhesive thickness. Given that the stiffnesses of the interface are decoupled from those of the bulk material, the interface stiffnesses are numerical parameters whose function is to ensure that the interface is rigidly bonded prior to damage. Opening interface stiffness is set arbitrarily high and shear interface stiffness is computed to fulfill Turon's constraint, i.e.

$$K_t^{(\text{int})} = K_n^{(\text{int})} \frac{G_{Ic}}{G_{IIc}} \left(\frac{\tau_t^0}{\tau_n^0}\right)^2 \tag{5}$$

where G_{Ic} and G_{IIc} are the opening and shear fracture toughnesses, respectively, and τ_n^0 and τ_t^0 are respectively the opening and shear interlaminar strengths [1].

The damage variable is a function of the interface-reduced displacement jumps, and is calculated using the cohesive element formulation of Turon et al. [3]. Because the interface-reduced displacement jumps are also a function of the current damage variable, as shown in Equations (1) and (2), an iterative loop is required to reach equilibrium. One pass of this loop involves calculating the interface-reduced displacement jump from the previous damage variable and updating the damage variable using the new interface-reduced displacement jump. Equilibrium is reached when the new interface-reduced displacement jump does not cause the damage variable to increase. It can be proven that convergence is guaranteed using this procedure for this particular case.

The formulation has been implemented as an Abaqus [4] user material subroutine.

2.2. Computational limitation of the adhesive thickness

The proposed cohesive element is intended to simulate thick adhesive interfaces with a single cohesive element along the adhesive layer thickness. Therefore, because the mesh is not refined along thickness direction, the element traction-separation response will have a snapback behavior for thicknesses greater than

$$t_{\max} = \frac{2\mathrm{G}_C E_{adh}}{\left(\sigma_n^{\max}\right)^2} \tag{6}$$

for pure mode I [5]. $t_{\max}$ is therefore proportional to Hillerborg's constant $\mathrm{G}_C E_{adh} / \left(\sigma_n^{\max}\right)^2$ [6], which is considered to be a material constant.

The snapback behavior implies that the damage state of the element suddenly changes from undamaged to totally damaged when its strength is reached. The fact that no partially damaged elements can exist means that the length of the numerical fracture process zone (FPZ) is essentially zero for $t \geq t_{max}$.

It is usually accepted [7] that at least three to five cohesive elements must be within the numerical FPZ length to accurately reproduce the interface behavior. In such cases where the element thickness is above $t_{\max}$ and the numerical fracture process zone length becomes zero, there is no mesh refinement that can achieve the previous condition and, therefore, the results might be inaccurate. In practice, Bazant and Oh [5] recommended the element thickness be below $t_{\max}/2$ for the crack band model. Given the similarity of the model proposed herein to the Bazant and Oh crack band model [5], the same threshold can be taken as a reference.

3. Finite element models and numerical results

3.1. Formulation validation

Numerical simulations of Double Cantilever Beam (DCB), End-Notched Flexure (ENF) and Mixed-Mode Bending (MMB) tests with different adhesive thicknesses have been conducted using the finite-thickness cohesive formulation proposed in this work. The geometry and properties of the simulated specimens were taken from [8], as well as the experimental results for comparison purposes. The specimens were 200 mm long and 25 mm wide. The two 2.5-mm-thick, carbon/epoxy adherents were co-bonded by means of a 0.254-mm-thick FM-300M adhesive layer with a pre-crack of 55 mm. The material and interface properties are detailed in Tables 1 and 2, respectively. The interface properties are directly obtained from the experimental tests in [8], with no further adjustment necessary. The specimens were modeled using the 2D, plane strain CPE4I Abaqus elements for the adherents and the COH2D4 Abaqus cohesive elements for the interface. The herein proposed cohesive element formulation was applied via a custom UMAT material subroutine. Regarding the mesh refinement, 0.1-mm-long cohesive elements were used to ensure that more than five elements are within the numerical FPZ [7]. The cohesive elements thickness was that of the adhesive layer.

E_{11} (GPa)	$E_{22}= E_{33}$ (GPa)	$G_{12} = G_{13}$ (GPa)	G_{23} (GPa)	$\nu_{12} = \nu_{13}$ (-)	ν_{23} (-)
142.0	7.8	4.0	2.8	0.34	0.40

Table 1. Elastic properties of the carbon/epoxy specimens (reproduced from [8]).

E_{adh} (MPa)	G_{adh} (MPa)	G_{Ic} (kJ/m^2)	G_{IIc} (kJ/m^2)	τ_n^{max} (MPa)	τ_t^{max} (MPa)	η (-)	$K_t^{(int)}$ (N/mm^3)
2921	1016	1.25	7.9	89.0	47.5	2.6	$2.25 \cdot 10^7$

Table 2. Interface properties of the FM-300M adhesive (reproduced from [8]). The Benzeggagh-Kenane mixed-mode interpolation parameter η [9] was assumed.

The results, shown in Figure 2, have been compared to LEFM closed-form solutions and to experimental results available in the literature for the ENF specimen. The results of the ENF specimen show an underestimation of the peak load with respect to the LEFM closed-form solution. However, the numerical results are in close agreement to the experimental data in [8] in terms of peak load. The FPZ was reported in [8] to be remarkably long in the ENF tests, which implies that LEFM assumptions do not hold and, therefore, LEFM results overestimate the peak load. The predicted peak load results provided by the proposed finite-thickness cohesive formulation for the ENF specimen are within 5% of the average experimental values regardless of the fracture process zone size. The predicted peak loads occur at lower displacements for the ENF specimens with thicker adhesive layers because of the added stiffness provided by the thicker adhesive layers.

The results are also shown to be in very good agreement with LEFM predictions for the DCB and the MMB 70% cases. The simulations of the DCB specimen were repeated with a different modeling technique. Instead of finite-thickness cohesive elements, the adhesive layer was modeled using two solid elements for the linear elastic behavior of the adhesive and a zero-thickness cohesive element [3] between them to simulate the interface fracture. The results were compared in terms of fracture process zone length to those obtained with the finite-thickness cohesive elements. In Figure 3, the normalized FPZ length with respect to the zero-thickness adhesive layer FPZ length is plotted against the normalized adhesive thickness with respect to the limit given by Equation (6).

It can be observed that the FPZ length of the finite-thickness cohesive element progressively decreases as the adhesive thickness grows, until $t_{\max}$ is reached. The FPZ length is zero thereafter, as expected. For the interface modeled using solid elements and zero-thickness cohesive elements, the thickness limitation is not observed. The differences observed in the FPZ lengths recovered using the two modeling techniques are in agreement with the recommendation given by Bazant and Oh of using element thicknesses below $t_{max}/2$ [5]. As can be observed from Figure 3, the difference in the numerical FPZ lengths for the DCB modeled using the two techniques is relatively low for adhesive thicknesses below $t_{max}/2$. All the simulations of the DCB, ENF, and MMB tests presented in Figure 2 were performed for a ratio t/t_{max} below 0.5.

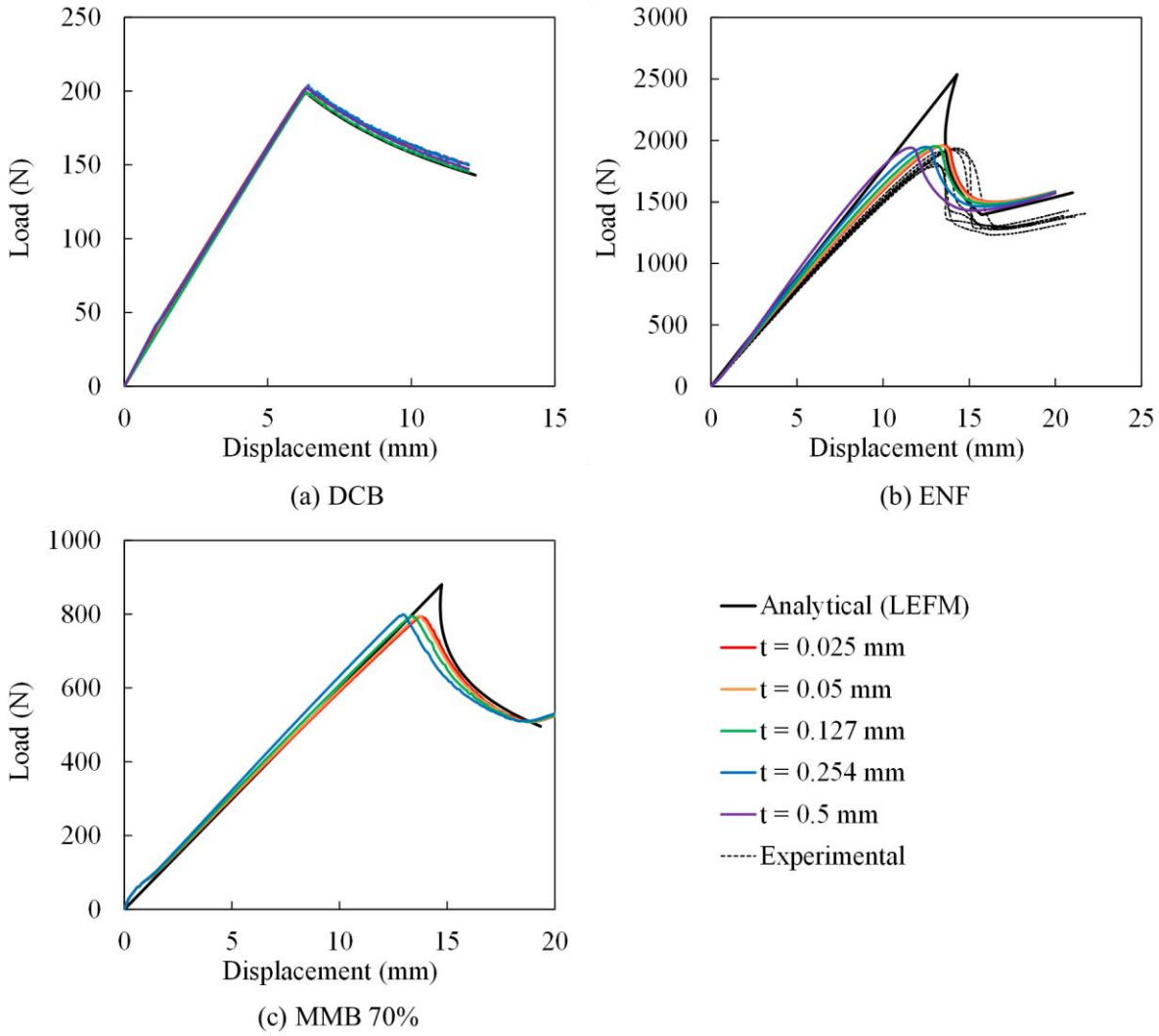

Figure 2. Force – displacement response of the DCB, ENF and MMB 70% tests with different adhesive thicknesses.

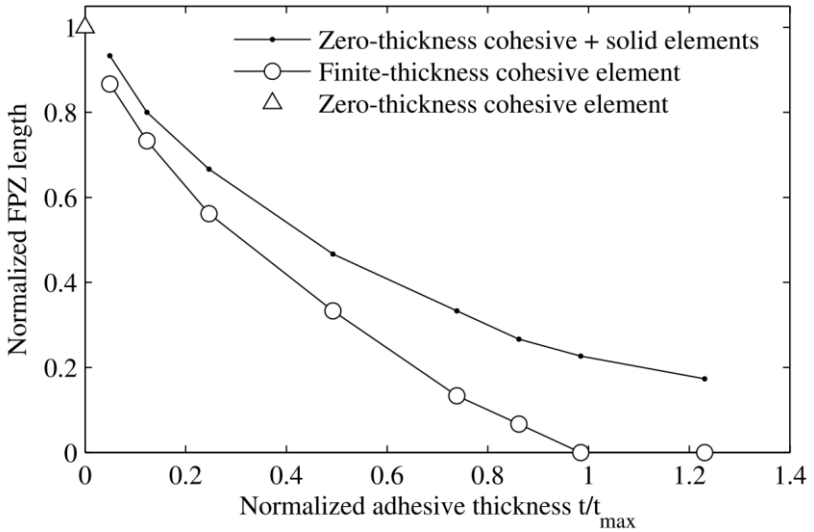

Figure 3. FPZ length as a function of the adhesive thickness for the DCB specimen. The FPZ length and the adhesive thickness have been normalized with respect to the FPZ length corresponding to the zero-thickness cohesive element and the maximum thickness of the element given by Equation (6), respectively.

3.2. Adhesive thickness effect on a SLJ specimen

The effect that the bondline thickness has on the structural response of a single lap joint has been studied using the proposed finite-thickness cohesive element. The experimental tests in [10] were simulated and the numerical and experimental results were compared.

The SLJ specimens were composed of two steel adherents joined with a Hysol EA9321 adhesive layer. The overlap length was 25 mm and specimens with adhesive layer thicknesses varying from 0.2 to 1.0 mm were tested. Each adherent was 95 mm long, 25 mm wide and 2 mm thick. The Young's modulus of the adherents was assumed to be 210 GPa and their Poisson ratio 0.3. The interface properties presented in Table 3 were directly taken from the experimental characterization in [10]. No further adjustment of these properties is needed to run the model. Regarding the finite element models, the 2D, plane strain CPE4I Abaqus element was used for the adherents and the proposed finite-thickness cohesive element was used for the adhesive. Cohesive elements with a length of 0.1 mm were used to ensure that more than five elements are within the numerical FPZ [7]. The cohesive elements' thickness was that of the adhesive layer.

$\mathbf{E_{adh}}$ (MPa)	$\mathbf{G_{adh}}$ (MPa)	G_{Ic} (kJ/m^2)	G_{IIc} (kJ/m^2)	$\boldsymbol{\tau_n^{max}}$ (MPa)	$\boldsymbol{\tau_t^{max}}$ (MPa)	η (-)	$\mathbf{K_t^{(int)}}$ (N/mm^3)
3870	1423	0.45	0.90	45.97	18.7	5.0	$1.2\cdot10^7$

Table 3. Interface properties of the Hysol EA9321 adhesive (reproduced from [10]). The Benzeggagh-Kenane mixed-mode interpolation parameter η [9] was assumed.

Both the experimental and the numerically predicted failure loads of the SLJ specimens are shown in Figure 4 as a function of the bondline thickness. The numerical results are in good agreement with the observed experimental behavior.

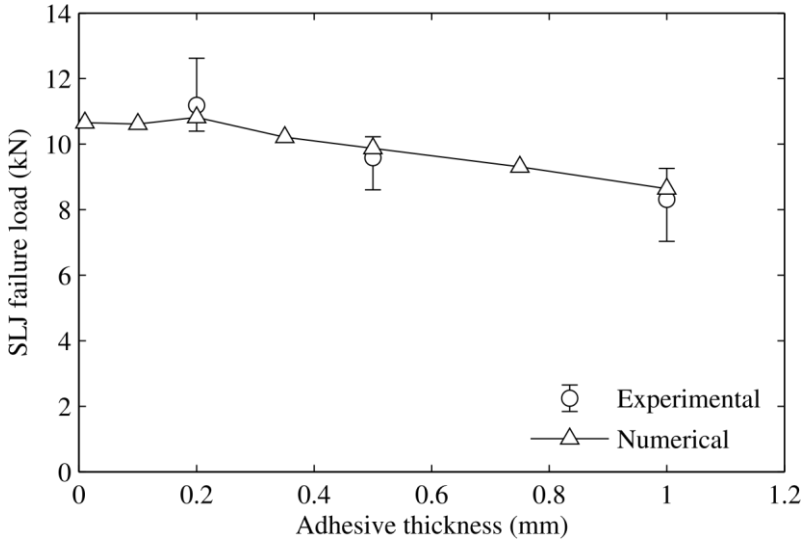

Figure 4. Experimental and numerical variation of the failure load of the SLJ specimen as a function of the adhesive thickness.

4. Conclusions

A new formulation for cohesive elements has been herein proposed that allows for a more accurate representation of the initial elastic response, softening, and ultimate failure of

adhesive materials with a finite thickness in a finite element model. The need for these modifications arose from Turon's observation that there exists a necessary constraint between the penalty stiffness, strength, and fracture toughness material properties of cohesive elements in order for fracture energy to be dissipated correctly [1]. To address this issue, the cohesive penalty stiffness and the physical adhesive stiffness were decoupled. The thick adhesive is considered as containing an embedded zero-thickness cohesive plane and stress equivalence is assumed between the bulk of the adhesive and across cohesive fracture plane. Good correlation was observed between model predictions and experimental data for DCB, ENF, MMB, and SLJ specimens. These predictions were achieved without any nonphysical material inputs required from the end user because Turon's constraint is internally satisfied within the cohesive element formulation.

The inclusion of progressive damage modeling methods in nonlinear finite element analyses often introduces a number of convergence related difficulties. For implicit analyses, the presence of the artificially high cohesive penalty stiffnesses in the global stiffness matrix often causes convergence problems. Likewise, the usage of very high penalty stiffnesses in explicit analyses often leads to prohibitively short minimum stable time increments. The decoupling of the physical and penalty stiffnesses in the herein proposed formulation removes the penalty stiffness from both the element and global stiffness matrices, addressing both of these issues.

References

[1] A. Turon, P. P. Camanho, J. Costa and J. Renart. Accurate simulation of delamination growth under mixed-mode loading using cohesive elements: Definition of interlaminar strengths and elastic stiffness. Composite Structures, 92(8): 1857–1864, 2010.

[2] C. Sarrado, A. Turon, J. Renart and I. Urresti. Assessment of energy dissipation during mixed-mode delamination growth using cohesive zone models. Composites Part A: Applied Science and Manufacturing, 43(11): 2128–2136, 2012.

[3] A. Turon, E. V. González, C. Sarrado, P. Maimí, Accurate simulation of delamination growth under mixed-mode loading using cohesive elements with mode-dependent penalty stiffness, to be submitted, 2014.

[4] ABAQUS version 6.12: ABAQUS User's Manual, SIMULIA World Headquarters, 166 Valley Street, Providence, RI 02909, USA, 2012.

[5] Z. P. Bazant and B. H. Oh. Crack band theory for fracture of concrete. Materials and Structures, 16: 155-177, 1983.

[6] A. Hillerborg, M. Modéer, P. E. Petersson. Analysis of crack formation and crack growth in concrete by means of fracture mechanics and finite elements. Cement and Concrete Research, 6: 773–82, 1976.

[7] A. Turon, C. G. Dávila, P. P. Camanho, J. Costa. An engineering solution for mesh size effects in the simulation of delamination using cohesive zone models. Engineering Fracture Mechanics, 74(10): 1665–1682, 2007.

[8] F. A. Leone, D. Girolamo, C. G. Dávila. Progressive Damage Analysis of Bonded Composite Joints. NASA/TM–2012-217790, 2012.

[9] M. L. Benzeggagh and M. Kenane. Measurement of mixed-mode delamination fracture toughness of unidirectional glass/epoxy composites with mixed-mode bending apparatus. Composites Science and Technology, 56(4): 439–449, 1996.

[10] L. F. M. da Silva, T. N. S. S. Rodrigues, M. A. V. Figueiredo, M. F. S. F. de Moura, J. A. G. Chousal. Effect of adhesive type and thickness on the lap shear strength. The Journal of Adhesion, 82: 1091-1115, 2006.